Article

Supercapacitor Performance of NiO, NiO-MWCNT, and NiO−Fe-MWCNT Composites

Aunggat Shah, Subhabrata Senapati, H C Ananda Murthy,* Laishram Robindro Singh, and Mrityunjoy Mahato*

Read Online

ACCESS | Metrics & More | Article Recommendations | Supporting Information

ABSTRACT: The NiO-CNT and NiO−Fe-CNT composites that have been prepared from waste high density polyethylene plastic and their carbon nanotube (CNT) quality-dependent super-capacitance tuning have been reported here. Multiwalled CNT (MWCNT) formation has been confirmed from TEM and Raman spectra with an I_D/I_G ratio of 0.77, which stands for high graphitization. The specific surface area (SSA) of MWCNTs in the NiO−Fe-CNT composite was 87.8 m^2/g, while in the NiO-CNT composite, it was 25 m^2/g. NiO−Fe-CNT displayed higher specific capacitance and energy density (1360 Fg^{-1} and 1180 W h kg^{-1}) than NiO-CNT (1250 Fg^{-1} and 1000 W h kg^{-1}), which may be due to the presence of higher-quality MWCNTs in the NiO−Fe-CNT composite. NiO−Fe-CNT displayed higher contributions of

electric double-layer capacitor (59%) behavior compared to NiO-CNT (38%) and represented a hybrid supercapacitor. NiO−Fe-CNT also displayed a capacitive retention of 96% after 1000 charge−discharge cycles. Furthermore, studies in acidic electrolytes revealed higher performance of NiO−Fe-CNT than NiO-CNT, displaying specific capacitances of NiO−Fe-CNT to be 1147 Fg^{-1} in 2 M H$_2$SO$_4$ and 943 Fg^{-1} in 2 M HCl. It has been qualitatively explored that the quality of CNTs, SSA, and quantum confinement effects in the composites may be the factors responsible for the performance difference in NiO−Fe-CNT and NiO-CNT. The present work is geared toward the low-cost fabrication of high-quality CNT composites for supercapacitors and energy storage applications. The present work also contributes quantitatively to the understanding of CNT quality as an important parameter for the performance of CNT-composite-based supercapacitors.
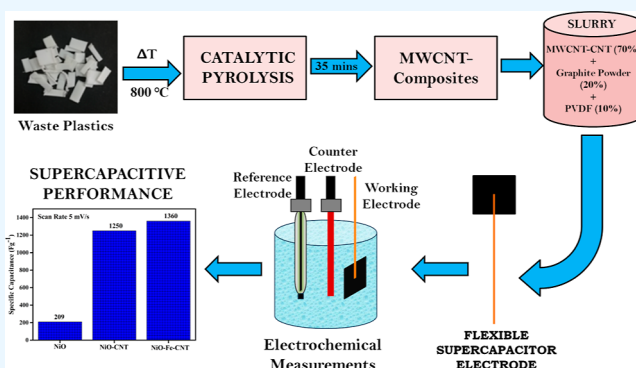
1. INTRODUCTION

Supercapacitors (SCs) are promising energy storage devices to deliver moderate energy densities and higher power densities and hence, SCs are another complimentary candidate along with the Li-ion batteries in energy storage devices.[1] SCs are attractive in many industries, such as automobiles, aerospace, electronics, and telecommunications.[2] The performance of SCs can be improved and optimized using nanofillers and nanocomposites. As per the nanotechnology principle, specific surface area (SSA) and quantum confinement effect are the contributing factors in enhancing any nanomaterial-based device. Also, the porosity of the nanostructure is also an added parameter specifically for energy storage devices such as SCs. Electrolytes can influence the storage performance of SCs by increasing ionic conductivity, redox reactions, charge transfer between electrodes, and double-layer formation for electric double-layer capacitors (EDLCs).[3] Electrochemical performance of SCs are defined by its various parameters, such as capacitance, energy density, power density, operating voltage, peak current, internal resistance, time constant, and cyclic stability/retention.[4]

CNTs are one of the promising carbon materials to be used as an electrode material in SCs due to their natural abundance, higher conductivity, higher SSA, porosity, etc.[5−7] CNTs can provide porous channels for electrolyte ions through their inner diameter to enhance their supercapacitive performance.[7] CNTs have higher SSA through their lower tube diameter (inner and outer diameters), which can reduce the separation between electrode−electrolyte boundaries, thus increasing the supercapacitive performance of SCs.[8] CNTs can be derived from renewable carbon sources, and hence, can be low-cost and environmentally friendly.[9−11] CNTs are ideal among the carbon materials for SC applications due to their high surface area and high thermal/chemical stability,[9−11] low electrolyte solution resistance or equivalent series resistance (ESR),

Table 1. Tabular Summary for Energy Storage Performance of NiO, NiO-CNT, and NiO−Fe-CNT Composites

| Sl. no	sample and source of CNT	source of CNT	NiO morphology	SC performance (C = F/g, E = W h/kg, P = W/kg, R = %)[a]	reference, year
1	NiO		quantum dot	C = 209, E = 153 P = 100 at 0.5 A/g, R = 98	present work
2	NiO-CNT	prepared from waste HDPE plastic carbon source	quantum dot	C = 1250, E = 1000 P = 100 at 0.5 A/g, R = 81	
3	NiO−Fe-CNT		nanoparticles	C = 1360, E = 1181 P = 100 at 0.5 A/g, R = 96	
4	NiO-CNT	purchased	nanoparticles	C = 879, E = 85 P = 1.6, R = 91	(2018)[19]
5	NiO-CNT			C = 622, E = N/R P = N/R, R = 100	(2016)[22]
6	NiO-CNT			C = 160, E = N/R P = N/R, R = 100	(2005)[59]
7	CNT-NiO			C = 523, E = N/R P = N/R, R = N/R	(2009)[60]
13	CNT-NiO		nano−micro flakes	C = 258, E = N/R P = N/R, R = 86	(2020)[61]
14	CNT-NiO			C = 258, E = N/R P = N/R, R = 86	(2013)[62]
8	GO/CNT/NiO		nanoflakes	C = 1180, E = N/R P = N/R, R = 95	(2014)[25]
9	NiO-CNT			C = 1727, E = N/R P = N/R, R = 91	(2014)[26]
10	CNT-NiO			C = 1511, E = N/R P = N/R, R = 92.4	(2014)[27]
11	CNT-NiO		nanosheets	C = 1844, E = 52.6 P = 219, R = 89	(2016)[23]
12	CNT-NiO			C = 996, E = 25.4 P = 400, R = 93	(2015)[24]
15	CNT-NiO		quantum dot (3.6 nm)	C = 2480, E = 21 P = 1100, R = N/R	(2016)[28]
16	NiO-CNT		porous micro-spheres	C = 1329, E = N/R P = N/R, R = 93	(2010)[21]

[a]N/R = Not reported.

porous structure, a wide range of band gap (0.18−1.8 eV), and tunable electrical properties.[12,13] A quantum confinement effect may also arise in CNTs from single-walled CNTs to multi-walled carbon nanotubes (MWCNTs), which may be an influential parameter for SC materials. CNTs are suitable for flexible electrodes due to their high strength, lightweight materials with Young's modulus of 1 TPa, and tensile strength of 63 GPa.[13,14] In this regard, quality of CNTs can also be a parameter to influence the storage performance of SCs, which has been reported in the present work.

A capacitor can store charge by transfer of electrons or faradaic processes or pseudocapacitance (PC), whereas an SC can store larger amounts of charges through additional non-faradaic processes, namely, electric double-layer (EDL) process, and hence SCs display higher specific capacitance, energy densities, and power densities.[15−17] The EDL process in SCs may be further improved by incorporating CNTs.[16,18] MWCNTs have been reported for SC application with specific capacitance in the range of 4−135 Fg^{-1}.[9] Hence, further enhancements in CNT-based EDLC SCs may be possible through their composite with metal oxides. It is reported that the metal oxides are pseudocapacitive in nature and hence, CNT−metal oxide composites can have both double-layer and pseudocapacitive storage mechanisms, i.e., function as a hybrid SC.[19] CNT−metal oxide composites can also prevent metal oxides from volume expansion upon repeated charge−discharge cycles and lead to the composite's higher stability.[20] The specific capacitances of NiO-CNT composites were reported for SC application by different researchers, such as 879 Fg^{-1} (Roy et al. by the co-precipitation method),[19] 1329 Fg^{-1} (Lin et al. by the co-precipitation method),[21] 622 Fg^{-1} (Yu et al. by the atomic layer deposition method),[22] and 1844 Fg^{-1} (Wen et al. by the electrostatic adsorption method).[23] Literature analysis of different NiO-CNT composites shows that their supercapacitive performance significantly depends on the morphology of NiO. The NiO-CNT composites having NiO as nanosheets,[23,24] nanoflakes,[25−27] porous nanoparticles,[21] and quantum-sized NiO particles,[28] (<10 nm) are

generally found to have increased supercapacitive performance (Table 1). The nanosheets, nanoflakes, and porous nanoparticles generally possess larger SSA, leading to larger electrochemically active sites, further leading to higher supercapacitive performance. Quantum-sized NiO particles as reported by Hakamada et al. 2016[28] showed that with the decrease in the size of NiO nanoparticles in the quantum region, there is a significant increase in the NiO-CNT composites' SC performance. However, no literature report tried to explore the reason for the variation of supercapacitive performance in the different NiO-CNT composites prepared through the same method.

The present work reports on the comparative SC performance of NiO, NiO-MWCNT, and NiO−Fe-MWCNT composites. A novel approach for a single-step preparation of NiO−Fe-CNT composites is reported using waste high-density polyethylene (HDPE) plastics with the application of a lab-developed pyrolysis reactor. The NiO−Fe-CNT composite was used to prepare polyethylene (PET)-based flexible electrodes for electrochemical analysis. The particle size of NiO in the NiO-CNT composite was in the 2−5 nm range (quantum dot range), whereas the particle size of NiO in NiO−Fe-CNT composite was in the 6−44 nm range. The number of walls, CNT diameter, density (2218 cm^{-3}), and the elastic modulus (28.63 GPa) of NiO−Fe-CNT composite have been reported in a previous work.[29] The Raman I_D/I_G ratio of 0.77 for NiO−Fe-CNT is indicative of low defect formation of MWCNTs as compared to the I_D/I_G ratio of 1.94 for NiO-CNT, which is indicative of the quality of CNTs and its structural integrity. The TEM images are complementary evidence for the direct observation CNT quality. Flexible SC electrodes were made using NiO-CNT and NiO−Fe-CNT as active materials on waste-derived PET sheets. The electrochemical measurements show a specific capacitance of 1360 Fg^{-1} for NiO−Fe-CNT and 1250 Fg^{-1} for NiO-CNT at 5 mVs^{-1} in a 2 M KOH electrolyte. The structural integrity and quality of CNTs have been tuned using ferrocene for CNT growth, which increases the energy density in NiO−Fe-CNT
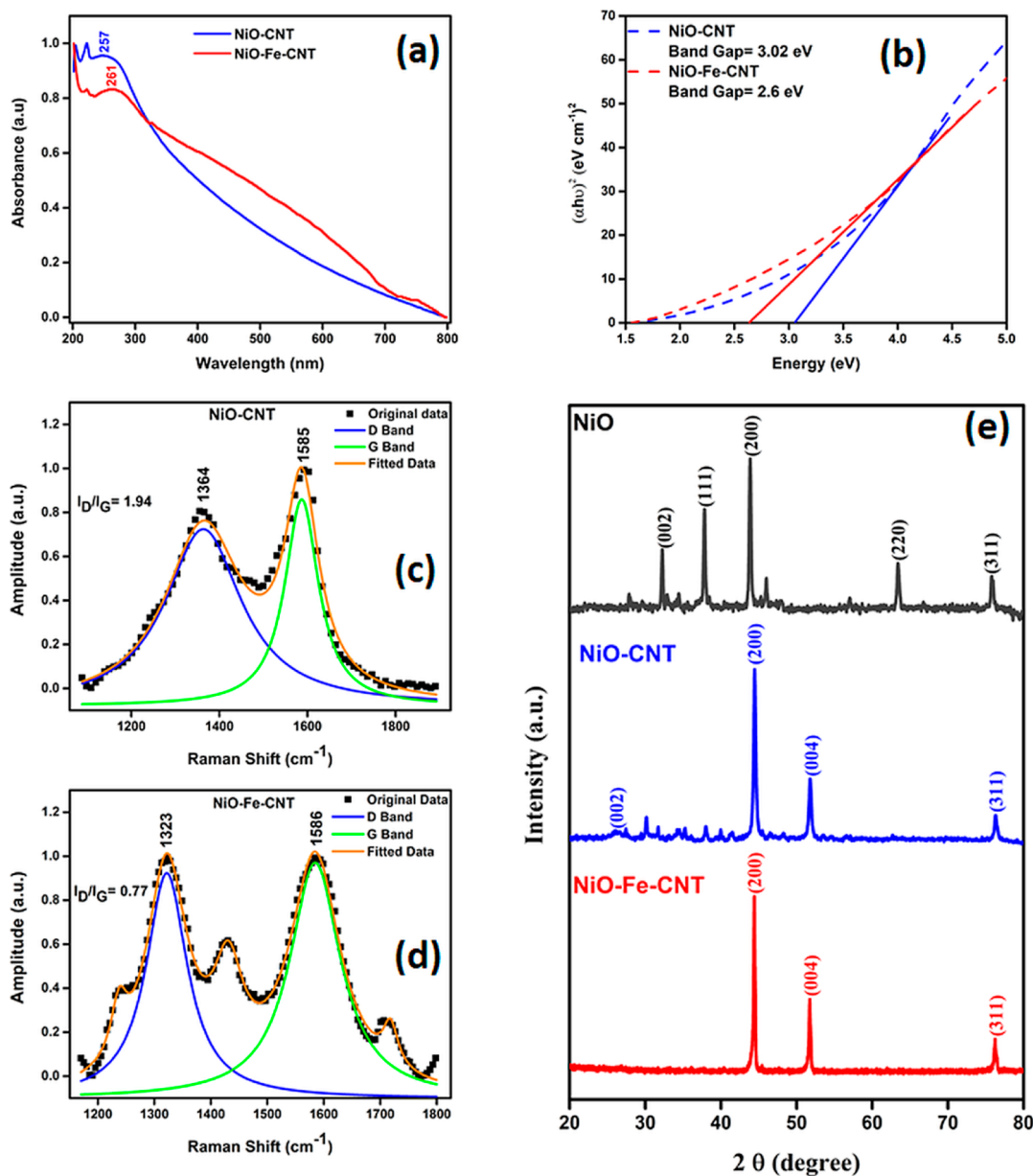
Figure 1. (a) UV−visible spectra of NiO-CNT and NiO−Fe-CNT. (b) Tauc plot of NiO-CNT and NiO−Fe-CNT and their band gaps' extrapolation. (c,d) Raman spectra of NiO-CNT and NiO−Fe-CNT. (e) Comparative XRD profile of NiO, NiO-CNT, and NiO−Fe-CNT.

to 1180 W h kg^{-1} as compared to 1000 W h kg^{-1} in NiO-CNT. Capacitive contributions were evaluated using the Trasatti method, and it was found that NiO−Fe-CNT displayed 59% EDLC behavior, 41% PC as compared to 38% EDLC, and 62% PC for NiO-CNT. NiO−Fe-CNT displayed enhanced EDLC behavior than NiO-CNT and acts as a high-performing hybrid SC electrode. NiO−Fe-CNT also showed higher stability than NiO-CNT in acidic electrolytes (2 M H_2SO_4 and 2 M HCl). The NiO−Fe-CNT displayed higher supercapacitive performance compared to NiO-MWCNTs, which may be attributed to its superior quality, lower defect, higher SSA, and quantum confinement effect owing to smaller tube thickness (∼8.5 nm) in NiO−Fe-CNT than in NiO-CNT.[30,31]

The higher supercapacitive performances of NiO−Fe-CNT composite material may arise due to the presence of higher quality of CNTs in the composite due to the use of ferrocene as the floating catalyst.[32,33] In the case of NiO−Fe-CNT and

NiO-CNT, the respective MWCNT diameters are 20.1 and 72.3 nm, with total wall thicknesses of 8.5 nm (NiO−Fe-CNT) and 24.65 nm (NiO-CNT). As a result, NiO−Fe-CNT is likely to experience stronger quantum confinement effects than NiO-CNT. The SSA of the MWCNT component within the composite is 87.8 m^2/g for NiO−Fe-CNT and 25 m^2/g for NiO-CNT. Thus, even though NiO-CNT (I_D/I_G = 1.94) possesses higher defects than NiO−Fe-CNT (I_D/I_G = 0.77), which contributes to the overall supercapacitive performance,[34] NiO−Fe-CNT displayed higher supercapacitive performance, which may be due to factors such as SSA, quality of CNTs, and quantum confinement effects in CNTs, leading to larger interfacial area for ion adsorption and desorption processes.[28,30,31]
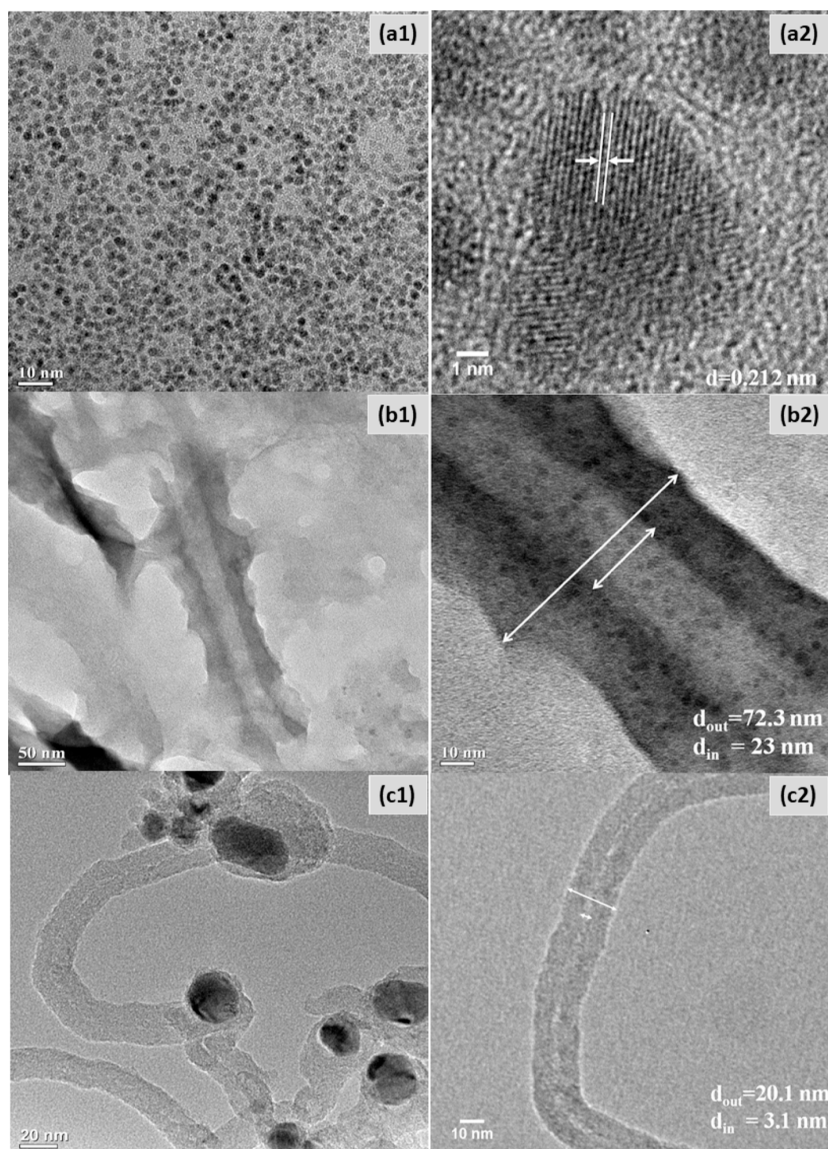
Figure 2. TEM images of NiO, NiO-CNT, and NiO−Fe-CNT at different scales: (a1,a2) NiO NP, (b1,b2) NiO-CNT, and (c1,c2) NiO−Fe-CNT.

2. RESULTS AND DISCUSSION

2.1. Material Characterizations by UV−Vis Absorption, TEM, XRD, and Raman Spectroscopy. UV−vis absorption spectra of NiO-CNT and NiO−Fe-CNT were obtained in ethylene glycol solvent. The absorption peak of NiO nanoparticles was found to be at 300 nm.[35] The absorption peak of NiO-CNT and NiO−Fe-CNT composites showed a blue shift to 257 and 261 nm, respectively, which may be due to the presence of CNTs (Figure 1a).[36] Jiang et al.[37] reported an absorption peak of CNTs at 253 nm and Cheng et al.[38] reported the characteristic absorption peak of MWCNTs in the range of 240−265 nm, which are in agreement with the present work.

The band gap of the prepared samples were determined by using Tauc's relation.[39,40]

$$\alpha h\nu = \alpha_0 (h\nu - E_g)^2 \tag{1}$$

The direct band gap of NiO nanoparticles is found to be 3.42 eV,[35,41] whereas the band gaps of NiO-CNT and NiO−Fe-CNT are found to be 3.02 and 2.6 eV, respectively (Figure

1b). The decrease in band gap in the composites is suggestive of CNT formation.[42] The CNTs are better acceptors of electrons, and hence it drives a small decrease in Fermi energy level during the composite formation. Figure S1a,b shows the powder sample images of NiO-CNT and NiO−Fe-CNT, respectively.

Raman spectra of NiO-CNT and NiO−Fe-CNT (Figure 1c,d) exhibited the two characteristic bands, D band and G band at 1364 and 1585 cm^{-1} for NiO-CNT, respectively, and at 1323 and 1586 cm^{-1} for NiO−Fe-CNT, respectively. The G band is due to in-plane vibrations of sp^2-bonded carbon atoms related to C−C stretching and is a measure of the degree of graphitization. The D band is due to the out-of-plane vibrations arising from the structural defects caused by the broken symmetry of the graphite unit cell.[43,44] The values of the I_D/I_G ratio are a measure of the disorder of the nanotube walls,[45] which is derived from the integrated area of deconvoluted Raman peaks and are found to be 1.94 for NiO-CNT and 0.77 for NiO−Fe-CNT. The lower value of I_D/I_G ratio of NiO−Fe-CNT (0.77) indicates the higher graphitization of NiO−Fe-CNT.
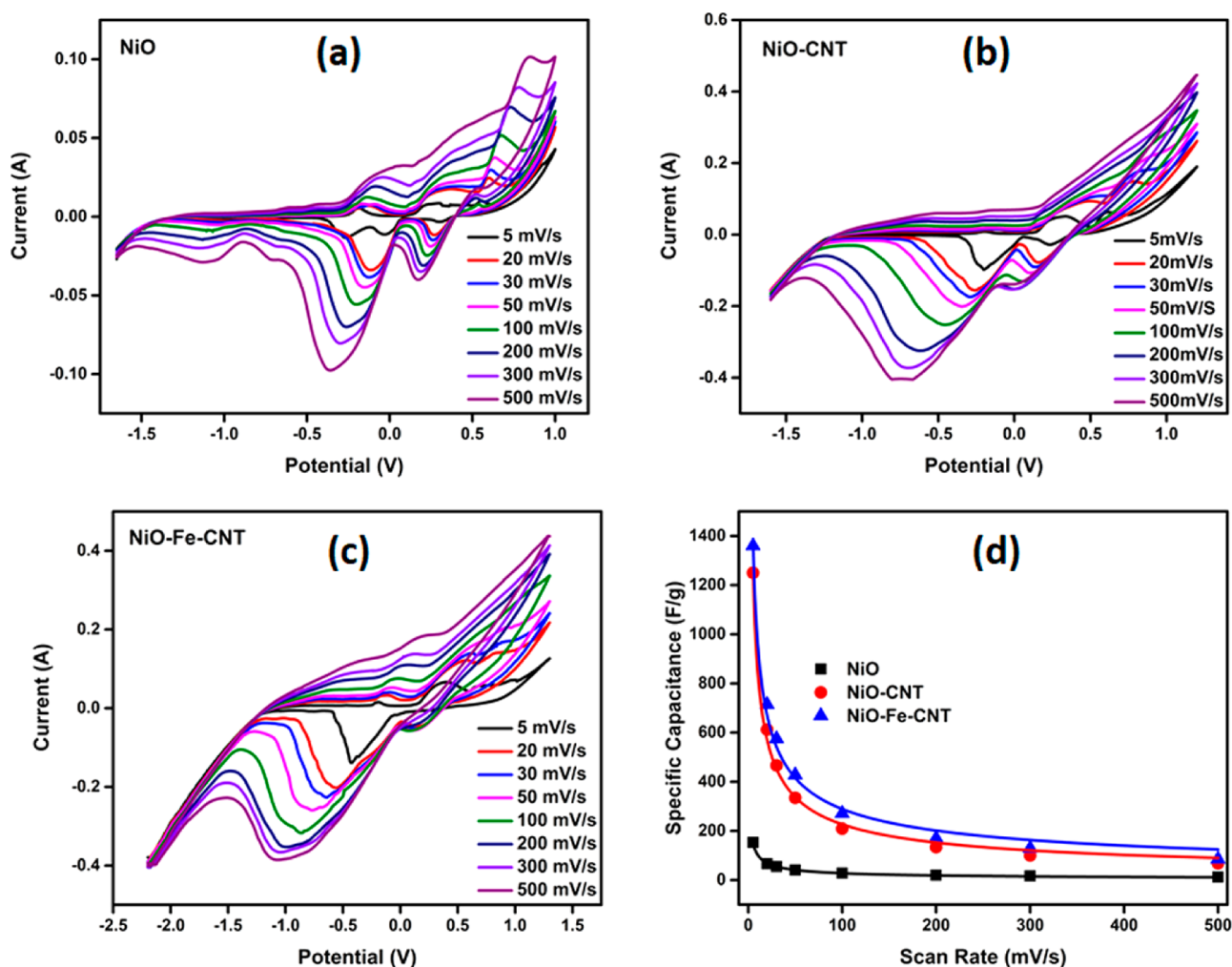
Figure 3. (a–c) Cyclic voltammetry curves of NiO, NiO-CNT, and NiO–Fe-CNT, respectively, at different scan rates. (d) Specific capacitance vs scan rate of different samples.

Figure 1e shows the XRD profiles of NiO, NiO-CNT, and NiO–Fe-CNT. The XRD patterns of NiO, NiO-CNT, and NiO–Fe-CNT contain major peaks at 26.12, 32.2, 37.8, 43.8, 52, 63.4, and 76° corresponding to planes at (002), (002), (022), (111), (004), (220), and (311), respectively.[40,46−49] The XRD peak at ∼ 44° corresponds to the (200) plane of NiO (JCPDS no. 47-1049).[40,50] The presence of XRD peaks at 26.12° (002) for NiO-CNT and 52° (004) for NiO–Fe-CNT confirms the presence of MWCNTs (JCPDS no. 75-1621).[51] It is to be noted that the peak at 26° was not observed in NiO–Fe-CNT, which may be due to the CNTs inside the composite and also due to the small scattering length of CNTs compared to metal (Ni) atoms.[52]

Figure 2a1,a2 shows TEM images of NiO nanoparticles and fringe patterns, respectively. The particle sizes of NiO-NPs were found to be in the range of 2−5 nm (Figure 2a1). The average d-spacing was calculated to be 0.212 nm, which corresponds to reflection from the (200) plane.[53] Figure 2b1,b2 shows TEM images of NiO-CNT showing tubular structures and confirming the formation of MWCNTs. Figure 2c1,c2 shows TEM images of NiO–Fe-CNT where the presence of tubular structures confirms CNT formation. The outer and inner diameters of MWCNTs were calculated using ImageJ software (Figure 2c2). They are as follows: NiO-CNT: d_{out} = 72.3 nm and d_{in} = 23 nm; NiO–Fe-CNT: d_{out} = 20.1 nm

and d_{in} = 3.1 nm. The number of walls of the CNTs was calculated as previously reported, using eq 2,[29,54] and found to be 74 for NiO-CNT and 26 for NiO–Fe-CNT.

$$n = \frac{1}{0.68 \text{ nm}}(d_{out} - d_{in}) \qquad (2)$$

The SSAs of NiO-CNT and NiO–Fe-CNT were studied using eq 3,[31] and they were found to be 25 and 87.8 m²/g, respectively, thus displaying higher surface area for NiO–Fe-CNT than NiO-CNT.

$$\text{SSA (MWCNT)} = \frac{1315 \times d_o}{nd_0 - 0.68[\sum_{i=1}^{n-1} i]} \qquad (3)$$

where 1315 is the theoretical SSA of SWCNT (in m²/g), d_o is the outer diameter of MWCNT, n is the no. of walls, 0.68 is the $2d_{s-s}$ (interlayer distance between successive walls), and $\sum_{i=1}^{n-1} i$ is the summation over no. of walls in the MWCNTs.

2.2. Electrochemical SC Characterizations. Electrochemical measurements were performed to determine the supercapacitive behavior of the three different electrodes (NiO, NiO-CNT, and NiO–Fe-CNT). The cyclic voltammetry and galvanostatic charge−discharge (GCD) measurements were carried out to evaluate the various parameters such as
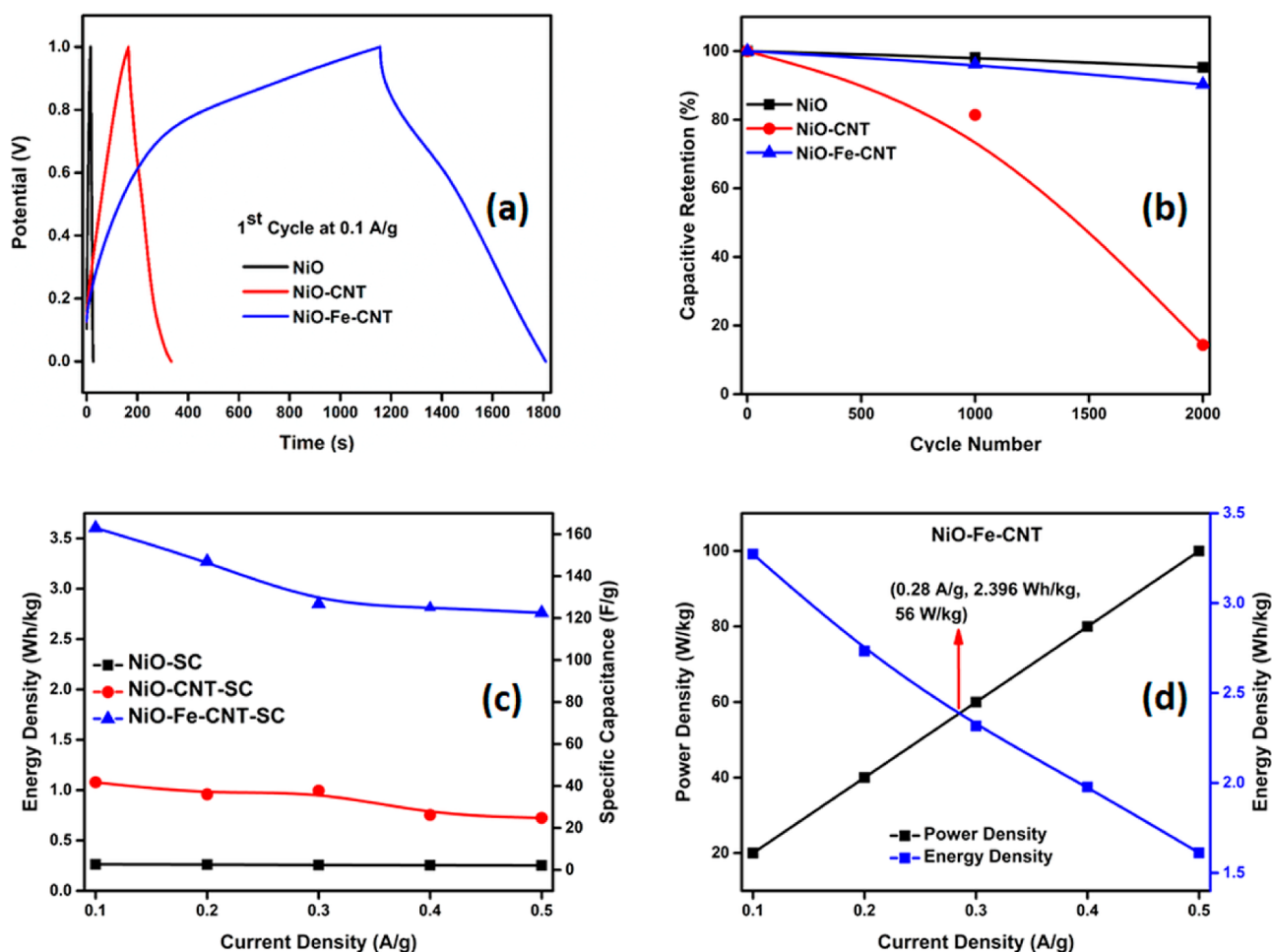
Figure 4. (a) Normalized GCD curves of NiO, NiO-CNT, and NiO−Fe-CNT of the 1st cycle at 0.1 Ag^{-1}. (b) Capacitive retention vs cycle number of the samples. (c) Energy density and specific capacitance at different current densities of the samples. (d) Plot for optimization of energy density, power density, and current density of NiO−Fe-CNT, obtained from GCD data.

specific capacitance (C_{sp} in Fg^{-1}), energy density (E in W h kg^{-1}), and power density (W kg^{-1}) using eqs 4−6.[55−57]

$$C_{sp} = \frac{1}{fm(V_f - V_i)} \int_{V_i}^{Vf} I(E) \, dE \tag{4}$$

$$E = \frac{1}{2}\left[C_{sp} \frac{(V_f - V_i)^2}{3.6} \right] \tag{5}$$

$$P = \frac{3600 \times E}{\Delta t} \tag{6}$$

where ΔV is the potential range, m is the mass of active material on electrodes, ν is the scan rate (mV s^{-1}), ($V_f - V_i$) is the sweeping potential range, $I(E)$ is the response current, and $\int_{V_i}^{Vf} I(E) \, dE$ is the area of the CV curves.[58]

Figure 3a−c shows cyclic voltammograms of NiO, NiO-CNT, and NiO−Fe-CNT recorded at different scan rates of 5−500 mV s^{-1}. The calculated specific capacitances for NiO, NiO-CNT, and NiO−Fe-CNT from CV at 5 mVs^{-1} were 209, 1250, and 1360 Fg^{-1}, respectively, and their respective energy densities of 153, 1000, and 1181 Wh kg^{-1} were in the order of NiO−Fe-CNT > NiO-CNT > NiO. The higher specific capacitances of CNT composites can be attributed to the presence of CNTs, which are in agreement with the lower

values of the band gap of CNT composites.[42] The higher capacitance of NiO−Fe-CNT than NiO-CNT is attributed to the higher quality of MWCNTs and surface area as evidenced from TEM and Raman spectra. An ideal EDLC is characterized by rectangular CV curves[9] and is reported the same in the case of carbon materials.[16]

The present CV curves (Figure 3a−c) show some deviations from an EDLC behavior, which may be due to the presence of NiO in the composites or silver paste in the final electrode. Therefore, the CV curves are indicative of a mixture of EDLC and pseudocapacitive behavior. Figure 3d shows the increase of specific capacitance at slower scan rates due to more time being available to the ions to percolate within the pores at a slow scan.[58] The lower scan rates allow the double-layer processes to contribute to the charge storage mechanism.[19] The lower scan rate region shows both faradaic and double-layer processes contributing to the charge storage mechanism.[19]

CV curves of bare PET with Cu wire, silver paste on PET with Cu wire, NiO, NiO-CNT, and NiO−Fe-CNT were taken for comparison at 500 mVs^{-1} (Figure S1c). The bare PET with Cu wire has a small CV area (0.02 VA) and silver paste-PET-Cu wire has a negligible CV area (0.038 VA) compared to the CV area of NiO−Fe-CNT (1.48 VA). Figure S1c indicates the 2.56% effect of silver paste in the electrochemical signal of the
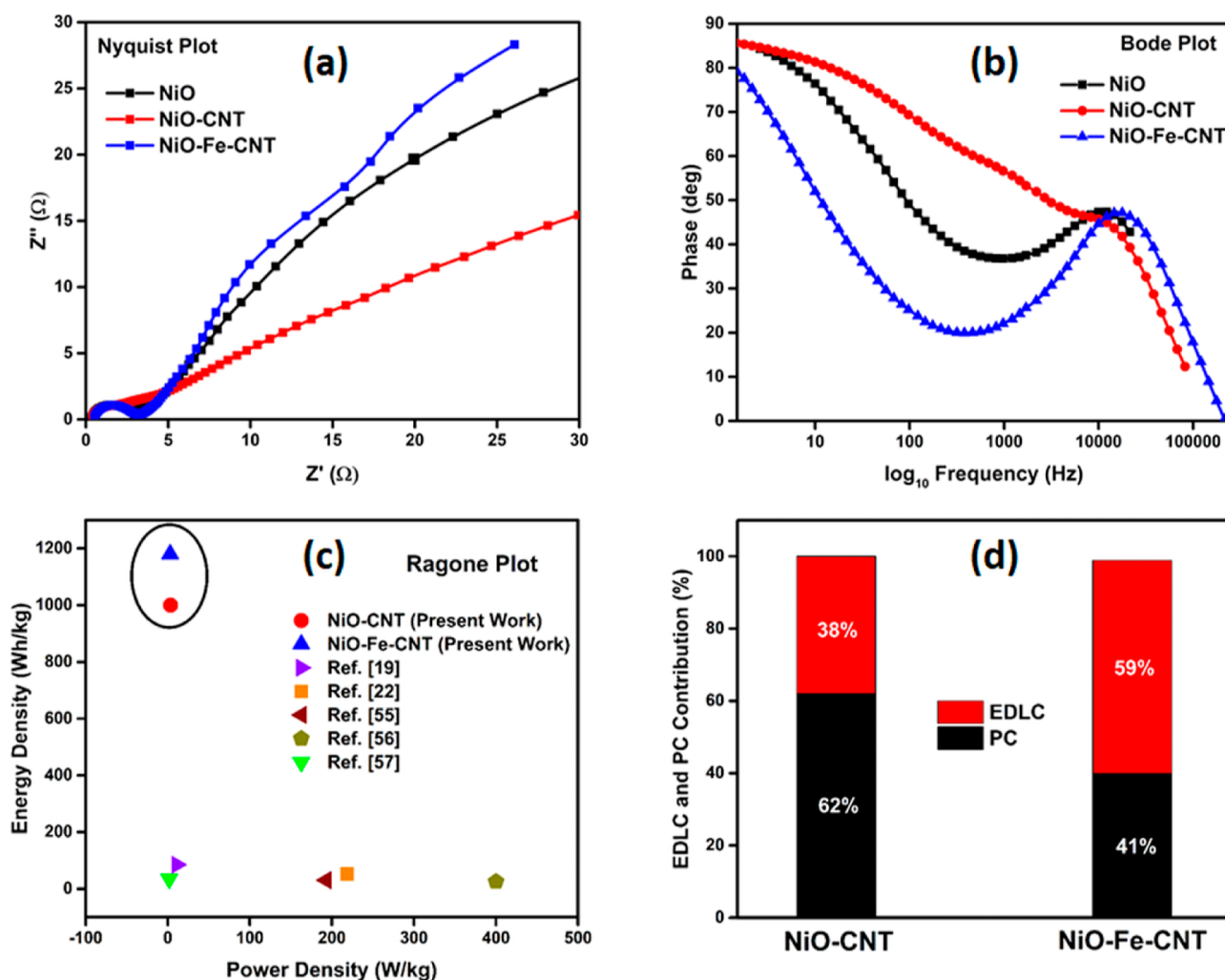
Figure 5. (a,b) Nyquist plot and Bode plot of the different samples (NiO, NiO-CNT, and NiO−Fe-CNT), respectively. (c) Ragone plot of the present work and reported literature of NiO-CNT-based composites, obtained from CV and Nyquist plot data. (d) Histograms for capacitive contribution (EDLC and PC) of NiO-CNT and NiO−Fe-CNT using the Trassati method.

prepared NiO−Fe-CNT electrode and also little contribution in the redox peaks.

GCD measurements were conducted using the chronopotentiometry method to further evaluate the performance of the electrode materials. The specific capacitances from charge−discharge measurements were calculated using eq 7.[16]

$$C_{sp} = \frac{I_m \Delta t}{\Delta V} \quad (7)$$

where I_m is the current density, Δt is the discharge time, and ΔV is the potential window.

Figure 4a shows normalized charge−discharge cycles of NiO, NiO-CNT, and NiO−Fe-CNT at a current density of 0.1 Ag^{-1}. The potential windows (ΔV) of NiO, NiO-CNT, and NiO−Fe-CNT electrodes were found to be 0.4 V. The specific capacitance of NiO−Fe-CNT have been calculated from GCD data (Figure 4a) to be 163 Fg^{-1} at 0.1 Ag^{-1}, whereas the specific capacitance of NiO and NiO-CNT were found to be 2.65 and 42 Fg^{-1}, respectively. The GCD data also suggest the better supercapacitive nature of NiO−Fe-CNT. The capacitive retentions of NiO−Fe-CNT, NiO-CNT, and NiO were found to be 96, 81, and 98%, respectively, at 1000 cycles and at 0.1 A/g, which shows better retention % of NiO−Fe-CNT

compared to NiO-CNT (Figure 4b). Figure S2 shows the GCD curves of NiO−Fe-CNT, NiO-CNT, and NiO at different current densities and different cycles, which are nearly symmetrical in nature and hence possess good capacitive behavior.[58]

Figure S3a,b shows capacitive retention at a higher current density, such as NiO−Fe-CNT having 59% at 0.5 Ag^{-1} and 2000 cycles and NiO-CNT having 14% at 0.5 Ag^{-1}. Figure S3c shows the bent image of the PET modified electrode indicating the flexible nature of the SC electrode. Figure 4c shows energy densities at different current densities of NiO, NiO-CNT, and NiO−Fe-CNT, respectively, showing the higher energy density of NiO−Fe-CNT. Figure S3d shows the energy density and power density of NiO−Fe-CNT up to the 2000th cycle, indicating high energy density retention after 2000 cycles. Figure 4d shows the optimum energy density, power density, and current density of the NiO−Fe-CNT SC to be 2.396 Wh kg^{-1}, 56 W kg^{-1}, and 0.28 Ag^{-1}, respectively. Figure S3e,f shows the optimum energy density, power density, and current density in the case of NiO and NiO-CNT, respectively.

Figure 5a shows the Nyquist plots of NiO, NiO-CNT, and NiO−Fe-CNT. The ESR is calculated from the cutting point of the Nyquist plot to the X-axis, which are found to be 0.38, 0.42, and 0.52 Ω, in the case of NiO, NiO-CNT, and NiO−Fe-
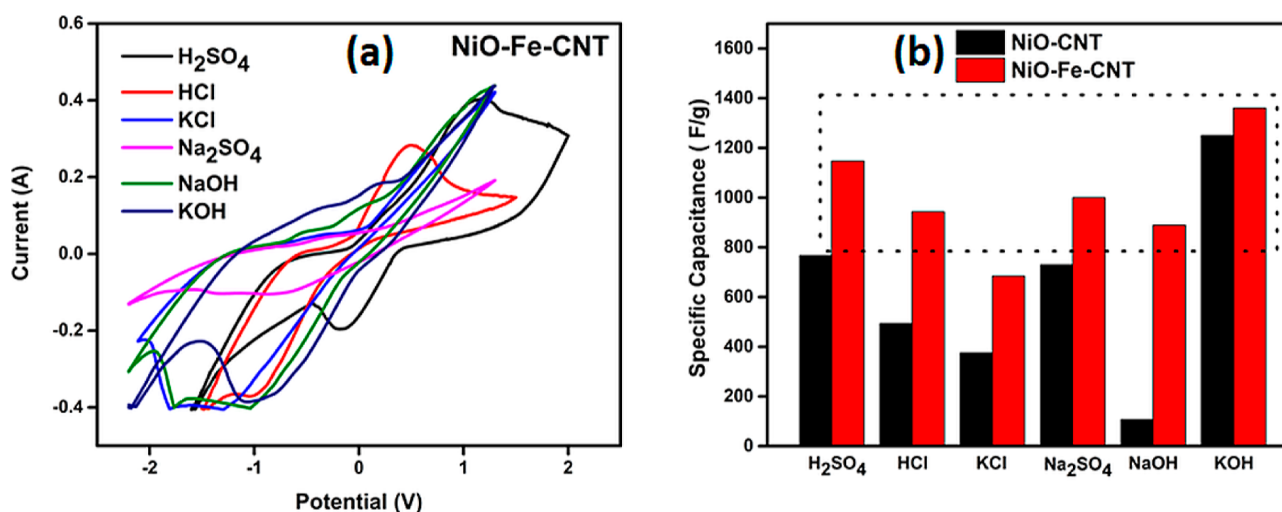
Figure 6. (a) CV curves NiO−Fe-CNT in different electrolytes. (b) Histogram of specific capacitance of NiO-CNT and NiO−Fe-CNT in different electrolytes.

CNT, respectively. Charge-transfer resistance (R_{CT}) or contact resistance between the electrode and the current collector is calculated from the diameter of the semicircle of the Nyquist plot[63] and found to be 2.72, 1.34, and 2.68 Ω for NiO, NiO-CNT, and NiO−Fe-CNT, respectively. Figure 5b shows the Bode plot (phase angles vs frequency) of NiO, NiO-CNT, and NiO−Fe-CNT to study the capacitive behavior at high frequencies. A SC's impedance may switch from pure capacitor to pure resistor with the variation of phase angle from 90 to 0°.[54] The capacitance is inversely proportional to frequency, and hence a SC theoretically behaves like a pure resistor at high frequencies with a near-zero phase angle.[55,58] Figure 5b indicates that the NiO, NiO-CNT, and NiO−Fe-CNT retain their capacitive nature at high frequencies up to a great extent. Figure 5c shows the Ragone plot of NiO−Fe-CNT as calculated using CV data and eq 8, which are compared with the reported literature.[64]

$$P = \frac{E^2}{4R_{ESR}} \qquad (8)$$

It is to be noted that the energy density of NiO−Fe-CNT has a quantum jump (>1000 W h kg^{-1}) compared to reported NiO-CNT-based composites (<100 W h kg^{-1}) though the specific capacitances are comparable with the literature (Table 1, Figure 5c). Figure S4 shows the Ragone plot of NiO, NiO-CNT, and NiO−Fe-CNT at different power densities, displaying the superior performance of NiO−Fe-CNT. The contributions of EDLC capacitance and PC of NiO-CNT and NiO−Fe-CNT have been calculated using the Trassati method (Figure 5d).[65] The total capacitance (C_T) and the EDLC capacitance (C_{EDLC}) have been calculated from the intercepts from the plots of $1/C$ vs $f^{1/2}$ and C vs $f^{-1/2}$, respectively, using eqs 9 and 10,[65] where f is the scan rate. Figure S5a,c is the plot of C^{-1} vs $f^{1/2}$ to calculate C_T, and Figure S5b,d is the plot of C vs $f^{-1/2}$ to calculate C_{EDLC} from intercepts of NiO-CNT and NiO−Fe-CNT, respectively. The EDLC behavior for NiO-CNT and NiO−Fe-CNT are valued at 38 and 62%, respectively, and PC contributions are 59 and 41%, respectively (Figure 5d). Figure 5d indicates an increase in EDLC behavior in NiO−Fe-CNT and behaves as a hybrid SC. The increase in EDLC behavior in NiO−Fe-CNT than in NiO-CNT can be attributed to the quality of the MWCNTs.

$$C^{-1} = \text{const} \, f^{0.5} + C_T^{-1} \qquad (9)$$

$$C = \text{const} \, f^{-0.5} + C_{EDLC} \qquad (10)$$

Therefore, the PC (C_{PC}) can be obtained from eq 11.[65]

$$C_T = C_{EDLC} + C_{PC} \qquad (11)$$

Figure 6a shows the cyclic voltammograms of NiO−Fe-CNT at 500 mV s^{-1} in different electrolytes (2 M H$_2$SO$_4$, HCl, KCl, Na$_2$SO$_4$, NaOH, and KOH), whereas Figure S6a shows the cyclic voltammograms of NiO-CNT. Figure 6b shows the specific capacitance of NiO-CNT and NiO−Fe-CNT in different electrolytes. It was found that NiO−Fe-CNT has a higher capacitance in all electrolytes (highlighted in the dotted rectangle) compared to NiO-CNTs, and it was also found that the optimized electrolyte was 2 M KOH. Figure S6b shows the largest potential window in 2 M KOH electrolytes for both NiO-CNT and NiO−Fe-CNT. Figure 6b also shows that NiO−Fe-CNT displayed higher specific capacitances in acidic electrolytes (1147 Fg^{-1} in H$_2$SO$_4$ and 943 Fg^{-1} in HCl) as compared to NiO-CNT (767 Fg^{-1} in H$_2$SO$_4$ and 494 Fg^{-1} in HCl), thus displaying higher stability of NiO−Fe-CNT in acidic electrolytes than NiO-CNT (as highlighted in the dotted rectangle). Figure S6b shows the wider potential window of NiO−Fe-CNT compared to NiO-CNT in different electrolytes, which also indicates higher stability.[66] Figure S6c,d shows the GCD profiles of NiO-CNT and NiO−Fe-CNT in different electrolytes, which indicates the negligible impact on GCD profiles in acidic electrolytes.

2.3. SC Performance of NiO−Fe-CNT vs NiO-CNT. The higher supercapacitive performances of the NiO−Fe-CNT composite material may have arisen due to the presence of higher quality of CNTs in the composite. Here, ferrocene has been used as a floating catalyst, which plays a vital role in higher graphitization and higher quality of CNTs in the NiO−Fe-CNT composite. The role of ferrocene in CNT quality is also evident in the literature; e.g., Lim et al.[32] observed longer CNTs using ferrocene with the nickel-doped Si substrate catalyst. Ferrocene decomposes to Fe particles as per eq 12,[33] which provides nucleation sites for carbon atoms for enhanced CNT growth.

$$Fe(C_5H_5)_2 \rightarrow Fe + 2C_5H_5 \qquad (12)$$

It is also to be noted that defect engineering in CNTs may increase its surface area and porosity to some extent and may influence the supercapacitive performance.[34] The Raman I_D/I_G ratio is a measure of defect of CNTs, and the NiO-CNT composite has higher defects (I_D/I_G = 1.94) than the NiO−Fe-CNT composite (I_D/I_G = 0.77). However, NiO−Fe-CNT displayed higher supercapacitive performance despite lower defects, which may be due to other factors such as SSA, quality of CNTs, and quantum confinement effects in CNTs, leading to larger interfacial area for ion adsorption and desorption processes.[28,31] CNTs may display quantum confinement effects along the radial direction in SWCNTs and MWCNTs (generally with a total wall thickness of <10 nm)[30] where the diameter of CNTs is twice the total wall thickness plus the inner diameter. The diameters of the MWCNTs in NiO−Fe-CNT and NiO-CNT are 20.1 and 72.3 nm, respectively, with total wall thicknesses of 8.5 nm (NiO−Fe-CNT) and 24.65 nm (NiO-CNT). Therefore, there may be higher quantum confinement effects in NiO−Fe-CNT than in NiO-CNT. It is also reported that the SSA is inversely proportional to the diameter of the CNTs, which can be calculated using eq 4 with the help of the outer diameter of the CNTs.[31] The SSAs of the MWCNT part within the composite are 87.8 and 25 m²/g for NiO−Fe-CNT and NiO-CNT, respectively. The higher SSA of NiO−Fe-CNT also facilitates more electrochemically active sites to be available to the electrolyte ions. Increased ion accessibility leads to improved ion transport kinetics, faster charge transfer, and higher capacitance. Thus, the quantum confinement effect, SSA, and quality of CNTs play crucial roles in increasing the performance of NiO−Fe-CNT as compared to NiO-CNT in otherwise similar NiO-CNT composites.

3. CONCLUSIONS

In the present work, we report for the first time a single-step synthesis of NiO−Fe-CNT from waste HDPE by a low-cost method to fabricate flexible SC electrodes. The formation of CNTs was confirmed from Raman spectra and TEM analysis. The NiO−Fe-CNT composite consisted of an average of 26 walls with outer and inner diameters of 20.1 and 3.1 nm, respectively, whereas NiO-CNT prepared without the use of ferrocene consisted of an average of 67 walls with outer and inner diameters of 72.3 and 23 nm, respectively. Also, the I_D/I_G ratio of 0.77 for NiO−Fe-CNT is indicative of low defect formation of MWCNTs as compared to the I_D/I_G ratio of 1.94 for NiO-CNT. Flexible SC electrodes were fabricated using NiO-CNT and NiO−Fe-CNT as active materials on waste PET sheets. From cyclic voltammetry analysis of the electrodes, specific capacitances of 1360 Fg⁻¹ for NiO−Fe-CNT and 1250 Fg⁻¹ for NiO-CNT at 5 mV s⁻¹ in 2 M KOH electrolyte were chosen. We observe that an increase in the structural integrity and quality of CNTs by the use of ferrocene for CNT growth directly results in an increase of specific capacitance and energy density of NiO−Fe-CNT. Despite lower defects in NiO−Fe-CNT, it displayed higher super-capacitive performance as compared to NiO-CNT, which may be due to the quality of CNTs, SSA, and quantum confinement effects. Capacitive contributions were evaluated using the Trassati method to evaluate the supercapacitive performance. We observed that NiO−Fe-CNT displayed 59% EDLC behavior and 41% PC as compared to 38 and 62% EDLC and PC, respectively, for NiO-CNT. The NiO−Fe-MWCNT electrodes displayed higher EDLC behavior, thus behaving more like a hybrid SC. The higher overall capacitance and

energy density of NiO−Fe-CNT are attributed to its better hybrid super capacitive nature than NiO-CNT. NiO−Fe-CNT also displayed a capacitive retention of 96% after 1000 charge−discharge cycles and 90% after 2000 cycles. To test the stability of the electrodes, electrochemical experiments were conducted in acidic electrolytes in which NiO−Fe-CNT again displayed higher stability than NiO-CNT in acidic electrolytes (2 M H_2SO_4 and 2 M HCl). NiO−Fe-CNT displayed specific capacitances of 1147 and 943 Fg⁻¹ in 2 M H_2SO_4 and 2 M HCl, respectively. Thus, we also observed higher stability of the NiO−Fe-CNT SC electrode in acidic electrolytes, and it also displayed significantly higher energy densities in acidic electrolytes than in NiO-CNT. The present work will thus contribute to the emerging field of low-cost production of CNTs. It will also quantitatively contribute to the under-standing of the effects of the quality of CNTs in composite materials for SC applications.

4. EXPERIMENTAL SECTION

4.1. Materials. Waste HDPE bottles were cut into pieces of 1 × 1 cm, cleaned, dried, and used to synthesize MWCNTs. Nickel acetate ($C_4H_6NiO_4 \cdot 4H_2O$, 98%), ethylene glycol ($HOCH_2CH_2OH$, 99%), sodium hydroxide (NaOH, 98%), ascorbic acid ($C_6H_8O_6$, 99.7%), and 1-methyl-pyrrolidine (NMP: $C_5H_{11}N$, 99.5%) were purchased from Merck India, polyvinylidene fluoride pellets (PVDF: ($C_2H_2F_2$)n, 180,000 by gel permeation chromatography) from Sigma-Aldrich, and ferrocene ($C_{10}H_{10}Fe$, 99%) from SRL. No further purification of chemicals was carried out, and all chemicals were used as received.

4.2. Preparation of NiO Nanoparticles. A nickel acetate solution (0.1 M) was prepared in ethylene glycol. An alkaline solution comprising ascorbic acid and NaOH with a molar ratio of 1:0.2 was prepared and added drop wise into the nickel solution under stirring till a green precipitate of $Ni(OH)_2$ (nickel hydroxide) was obtained. The precipitate was filtered and washed several times by DI water followed by ethanol. Finally, it was calcined at 400 °C for a duration of 6 h and NiO grayish-black nanoparticle powder was collected.[21,29,67]

4.3. Preparation of NiO-MWCNT. Synthesis of NiO-MWCNT composites was carried out via pyrolysis of waste HDPE plastics in a custom-made two-stage "pyrolysis reactor furnace"[68] as reported in earlier works.[29,35,55] NiO catalysts were kept in a silica bed in the second reactor, and HDPE plastics were kept in a porcelain bed in the first reactor. The ratio of plastic and catalyst was kept as 1:1, and the furnace was made inert by N_2 gas with a flow rate of 100 mL/min during the entire process, which also acted as a carrier gas to carry hydrocarbons to the second reactor. The first reactor was heated to 600 °C (heating rate = 10 °C/min) to initiate the pyrolysis process, and the second reactor was heated to 800 °C (heating rate = 10 °C/min) for thermocatalytic decomposition of hydrocarbons and subsequent growth of MWCNTs. The reactor was heated for 35 min to maintain the temperature and allowed to cool down gradually.

4.4. Novel One-Step Synthesis of NiO−Fe-CNT. A novel one-step synthesis of NiO−Fe-CNT was carried out for the first time by pyrolysis of waste HDPE plastics in a custom-made two-stage pyrolysis reactor furnace.[68] However, one of the two reactors was employed during the entire process. The pyrolysis of waste HDPE plastic and its decomposition were carried out in a single step to grow MWCNTs.

200 mg of the NiO nanocatalyst, 200 mg of ferrocene, and 400 mg of waste HDPE plastics were kept together on a silica boat. The silica boat was placed inside the reactor, and N_2 gas was passed to replace the oxygen and make the inert atmosphere. The N_2 flow was maintained for 20 min, and the reactor was heated to 800 °C. A static N_2 environment was maintained instead of constant gas flow in order to avoid the displacement of hydrocarbons from being available to the catalysts for MWCNT growth. The temperature was maintained for 35 min, and the reactor was allowed to cool down gradually.

4.5. PET-Modified Electrode Preparation. A novel paint-cast method was used for the preparation of flexible SC electrodes. 1 × 1 cm of consumer-grade PET sheets were cleaned with distilled water followed by ethanol under sonication. Cu wires were passed through the center of the PET sheets and was washed again in an ultrasonicator.

Active material, graphite powder, and PVDF were mixed in a 7:2:1 ratio to form the electrode slurry, which was then sonicated for 4 h.[16] The PET sheet was painted with the slurry using a paintbrush, i.e., the paint-cast method and dried for 30 min at 50 °C in a hot air oven. The paint cast method was repeated 5−6 times to get a uniform coating. The junction between the PET sheet and Cu wire was filled up using silver conducting paste to make it more conducting (contact resistance ∼0.5−1.5 Ω). The final electrode was dried in a hot air oven for 3 h at 50 °C and subsequently used for electrochemical measurements.

4.6. UV−visible Spectra and Raman Spectra Characterization. A UV−visible absorption spectrophotometer (model: Hitachi U-3900) was used for measuring the UV−visible spectra of NiO, NiO-CNT, and NiO−Fe-CNT. The spectrophotometer had a double beam and a single monochromator, and experiments were performed with scan rates of 1−2400 nm/min, a wavelength range of 190−900 nm, with an accuracy of 0.1 nm. The deuterium lamp for UV range and 50 W tungsten iodide for visible range were used. A quartz cuvette (path length of 10 mm) was used as a sample container.

A laser micro Raman system (make: Horiba Jobin Vyon, Model: LabRam HR) using a diode laser (485 nm) and equipped with a liquid nitrogen cooling arrangement was used to carry out Raman spectroscopic measurements.

4.7. TEM and XRD Characterization. TEM images of the catalyst and the composite were recorded using TEM (make: JEOL, model: JEM-2100) with an accelerating voltage of 60−200 kV in 50 V steps with a resolution of 1.9 to 1.4 Å (lattice) and an achievable magnification of 50× to 1,500,000×.

XRD data of the NiO and CNT composites were taken by a Rigaku X-ray diffractometer (make: Rigaku, Model: TTRAX-III 18 kW) using Cu Kα (λ = 1.5406 Å) radiation at a range of 2θ = 20−80°.

4.8. Electrochemical Measurements. Electrochemical measurements (cyclic voltammetry, GCD, and EIS) of NiO, NiO-MWCNT, and NiO−Fe-MWCNT were conducted using an electrochemical workstation (CH Instrument Model: CHI660D). The electrodes used were platinum wire (counter electrode), Ag/AgCl (reference electrodes), and PET modified with active material (working electrode). The CV data were repeated in different electrolytes of a 2 M concentration (KOH, H_2SO_4, HCl, KCl, Na_2SO_4, and NaOH) at scan rates 5−500 mV s^{-1}, and the 2 M KOH electrolyte was optimized. GCD measurements were conducted by using the chronopo-

tentiometry method where the upper and lower potential limits were taken to be ±20% of the open-circuit potential. EIS was conducted in 2 M KOH in the range of 1−100,000 Hz, where the starting potential was taken to be approximately the open-circuit potential.

■ ASSOCIATED CONTENT

ⓈI Supporting Information

The Supporting Information is available free of charge at https://pubs.acs.org/doi/10.1021/acsomega.3c03044.

> Powder samples of NiO-CNT and NiO−Fe-CNT; comparative CV curves of bare PET with Cu wire and different modified PET; GCD cycles of NiO−Fe-CNT and NiO at different current densities and different cycles; capacitive retention of NiO-CNT and NiO−Fe-CNT; energy density vs power density plot of NiO−Fe-CNT; Ragone plot (energy density vs power density) of NiO, NiO-CNT, and NiO−Fe-CNT, obtained from CV data; and Trassati plot for capacitance contribution for EDLC and PC in different samples of NiO-CNT and NiO−Fe-CNT (PDF)

■ AUTHOR INFORMATION

Corresponding Authors

H C Ananda Murthy − *Department of Applied Chemistry, School of Applied Natural Science, Adama Science and Technology University, 1888 Adama, Ethiopia; Department of Prosthodontics, Saveetha Dental College & Hospital, Saveetha Institute of Medical and Technical Science (SIMATS), Saveetha University, Chennai, Tamil Nadu 600077, India;* ◉ orcid.org/0000-0002-2361-086X; Email: mrityunjoyphy1@gmail.com

Mrityunjoy Mahato − *Physics Division, Department of Basic Sciences and Social Sciences, School of Technology, North-Eastern Hill University, Shillong, Meghalaya 793022, India;* Email: anandkps350@gmail.com

Authors

Aunggat Shah − *Physics Division, Department of Basic Sciences and Social Sciences, School of Technology, North-Eastern Hill University, Shillong, Meghalaya 793022, India*

Subhabrata Senapati − *Physics Division, Department of Basic Sciences and Social Sciences, School of Technology, North-Eastern Hill University, Shillong, Meghalaya 793022, India*

Laishram Robindro Singh − *Department of Nanotechnology, School of Technology, North Eastern Hill University, Shillong, Meghalaya 793022, India*

Complete contact information is available at:
https://pubs.acs.org/10.1021/acsomega.3c03044

Author Contributions

AS took part in the experimentation, data analysis, and drafting of the manuscript. SS performed the experimentation. LRS carried out the reviewing and data recording. HCAM participated in the review/editing. MM executed the project administration, data analysis, and the final manuscript. All authors read the manuscript in detail and approved the final version.

Notes

The authors declare no competing financial interest.

ACKNOWLEDGMENTS

REFERENCES

(1) Senthil, T.; Divakaran, N.; Kale, M. B.; Mubarak, S.; Dhamodharan, D.; Wu, L.; Bensingh, R. J.; Kader, M. A.; Dutta, K. Low-dimensional carbon-based nanomaterials for energy conversion and storage applications. In *Nanostructured, Functional, and Flexible Materials for Energy Conversion and Storage Systems*; Pandikumar, A., Rameshkumar, P., Eds.; Elsevier, 2020; pp 15−68. DOI: DOI: 10.1016/B978-0-12-819552-9.00002-6.

(2) Kötz, R.; Carlen, M. Principles and applications of electrochemical capacitors. *Electrochim. Acta* 2000, 45, 2483−2498.

(3) Saikia, B. K.; Benoy, S. M.; Bora, M.; Tamuly, J.; Pandey, M.; Bhattacharya, D. A brief review on supercapacitor energy storage devices and utilization of natural carbon resources as their electrode materials. *Fuel* 2020, 282, 118796.

(4) Zhang, S.; Pan, N. Supercapacitors Performance Evaluation. *Adv. Energy Mater.* 2015, 5, 1401401.

(5) Snook, G. A.; Kao, P.; Best, A. S. Conducting-polymer-based supercapacitor devices and electrodes. *J. Power Sources* 2011, 196, 1−12.

(6) Samuel, J.; Shah, A.; Kumar, D.; Singh, L. R.; Mahato, M. Preparation, characterization and some electrochemical study of waste derived iron Oxide-Carbon nanocomposite. *Mater. Today: Proc.* 2021, 47, 1048−1053.

(7) Das, H. J.; Shah, A.; Singh, L. R.; Mahato, M. Waste derived low cost PbO-Carbon nanocomposite and its energy storage application. *Mater. Today: Proc.* 2021, 47, 1072−1077.

(8) Hillier, N.; Yong, S.; Beeby, S. The good, the bad and the porous: A review of carbonaceous materials for flexible supercapacitor applications. *Energy Rep.* 2020, 6, 148−156.

(9) Frackowiak, E.; Béguin, F. Carbon materials for the electrochemical storage of energy in capacitors. *Carbon* 2001, 39, 937−950.

(10) Xie, L.; Sun, G.-H.; Su, F.; Guo, X.; Kong, Q.; Li, X.; Huang, X.; Wan, L.; Song, W.; Li, K.; et al. Hierarchical porous carbon microtubes derived from willow catkins for supercapacitor applications. *J. Mater. Chem.* 2016, 4, 1637−1646.

(11) Forouzandeh, P.; Kumaravel, V.; Pillai, S. C. Electrode Materials for Supercapacitors: A Review of Recent Advances. *Catalysts* 2020, 10, 969−1041.

(12) Cheng, Q.; Tang, J.; Ma, J.; Zhang, H.; Shinya, N.; Qin, L. C. Graphene and carbon nanotube composite electrodes for supercapacitors with ultra-high energy density. *Phys. Chem. Chem. Phys.* 2011, 13, 17615−17624.

(13) Shah, A.; Saha, G.; Mahato, M. Parameters Involved in CVD Growth of CNT: A Review. In *Tailored Functional Materials*; Mukherjee, K., Layek, R. K., De, D., Eds.; *Springer Proceedings in Materials*; Springer, 2022; pp 185−198.

(14) Saifuddin, N.; Raziah, A. Z.; Junizah, A. R. Carbon Nanotubes: A Review on Structure and Their Interaction with Proteins. *J. Chem.* 2013, 2013, 1−18.

(15) Gautham Prasad, G.; Shetty, N.; Thakur, S.; Rakshitha; Bommegowda, K. B. Supercapacitor technology and its applications: a review. *IOP Conf. Ser.: Mater. Sci. Eng.* 2019, 561, 012105.

(16) Aboutalebi, S. H.; Chidembo, A. T.; Salari, M.; Konstantinov, K.; Wexler, D.; Liu, H. K.; Dou, S. X. Comparison of GO, GO/MWCNTs composite and MWCNTs as potential electrode materials for supercapacitors. *Energy Environ. Sci.* 2011, 4, 1855−1865.

(17) Ciocan, I.; Fǎrcǎ, C.; Grama, A.; Tulbure, A. An Improved Method for the Electrical Parameters Identification of a Simplified PspiceSupercapacitor Model. *2016 IEEE 22nd International Symposium for Design and Technology in Electronic Packaging (SIITME)*, 2016; pp 171−174.

(18) Jian, X.; Li, H.; Li, H.; Li, Y.; Shang, Y. Flexible and freestanding MoS_2/rGO/CNT hybrid fibers for high-capacity all-solid supercapacitors. *Carbon* 2021, 172, 132−137.

(19) Roy, A.; Ray, A.; Saha, S.; Ghosh, M.; Das, T.; Satpati, B.; Nandi, M.; Das, S. NiO-CNT composite for high performance supercapacitor electrode and oxygen evolution reaction. *Electrochim. Acta* 2018, 283, 327−337.

(20) An, C.; Zhang, Y.; Guo, H.; Wang, Y. Metal oxide-based supercapacitors: progress and prospectives. *Nanoscale Adv.* 2019, 1, 4644−4658.

(21) Lin, P.; She, Q.; Hong, B.; Liu, X.; Shi, Y.; Shi, Z.; Zheng, M.; Dong, Q. The Nickel Oxide/CNT Composites with High Capacitance for Supercapacitor. *J. Electrochem. Soc.* 2010, 157, A818.

(22) Yu, L.; Wang, G.; Wan, G.; Wang, G.; Lin, S.; Li, X.; Wang, K.; Bai, Z.; Xiang, Y. Highly effective synthesis of NiO/CNT nanohybrids by atomic layer deposition for high-rate and long-life supercapacitors. *Dalton Trans.* 2016, 45, 13779−13786.

(23) Wen, Z. B.; Yu, F.; You, T.; Zhu, L.; Zhang, L.; Wu, Y. P. A core−shell structured nanocomposite of NiO with carbon nanotubes as positive electrode material of high capacitance for supercapacitors. *Mater. Res. Bull.* 2016, 74, 241−247.

(24) Yi, H.; Wang, H.; Jing, Y.; Peng, T.; Wang, X. Asymmetric supercapacitors based on carbon nanotubes@NiO ultrathin nanosheets core-shell composites and MOF-derived porous carbon polyhedrons with super-long cycle life. *J. Power Sources* 2015, 285, 281−290.

(25) Bai, Y.; Du, M.; Chang, J.; Sun, J.; Gao, L. Supercapacitors with high capacitance based on reduced graphene oxide/carbon nanotubes/NiO composite electrodes. *J. Mater. Chem. A* 2014, 2, 3834−3840.

(26) Gund, G. S.; Dubal, D. P.; Shinde, S. S.; Lokhande, C. D. Architectured Morphologies of Chemically Prepared NiO/MWCNTs Nanohybrid Thin Films for High Performance Supercapacitors. *ACS Appl. Mater. Interfaces* 2014, 6, 3176−3188.

(27) Wu, M.-S.; Zheng, Y.-R.; Lin, G.-W. Three-dimensional carbon nanotube networks with a supported nickel oxide nanonet for high-performance supercapacitors. *Chem. Commun.* 2014, 50, 8246−8248.

(28) Hakamada, M.; Abe, T.; Mabuchi, M. Electrodes from carbon nanotubes/NiO nanocomposites synthesized in modified Watts bath for supercapacitors. *J. Power Sources* 2016, 325, 670−674.

(29) Senapati, S.; Shah, A.; Patra, P. K.; Mahato, M. Measurement of elastic modulus of CNT composites: a nondestructive study. *Fullerenes, Nanotubes Carbon Nanostruct.* 2021, 30, 290−296.

(30) Chico, L.; Jaskolski, W.; Sancho, M. L.; Munoz, M. Quantum confinement in carbon-nanotube systems. *Internet J. Nanotechnol.* 2005, 2, 103−113.

(31) Peigney, A.; Laurent, C.; Flahaut, E.; Bacsa, R. R.; Rousset, A. Specific surface area of carbon nanotubes and bundles of carbon nanotubes. *Carbon* 2001, 39, 507−514.

(32) Lim, Y. D.; Avramchuck, A. V.; Grapov, D.; Tan, C. W.; Tay, B. K.; Aditya, S.; Labunov, V. Enhanced Carbon Nanotubes Growth Using Nickel/FerroceneHybridized Catalyst. *ACS Omega* 2017, 2, 6063−6071.

(33) Samandari-Masouleh, L.; Mostoufi, N.; Khodadadi, A.; Mortazavi, Y.; Maghrebi, M. Modeling the Growth of Carbon Nanotubes in a Floating Catalyst Reactor. *Ind. Eng. Chem. Res.* 2012, 51, 1143−1149.

(34) Yun, Y. S.; Yoon, G.; Kang, K.; Jin, H.-J. High-performance supercapacitors based on defect-engineered carbon nanotubes. *Carbon* 2014, 80, 246−254.

(35) Nath, A.; Shah, A.; Singh, L. R.; Mahato, M. Waste plastic-derived NiO-MWCNT composite as visible light photocatalyst for degradation of methylene blue dye. *Nanotechnol. Environ. Eng.* 2021, 6, 70.

(36) George, R.; Kumar, L. A.; Alagappan, M. Synthesis of nanotubular nio-cnt composite and its application in temperature independent CO_2 gas sensors fabricated using interdigitated silver electrode. *Dig. J. Nanomater. Biostruct.* 2019, 14, 213−224.

(37) Jiang, L.; Gao, L.; Sun, J. Production of aqueous colloidal dispersions of carbon nanotubes. *J. Colloid Interface Sci.* **2003**, *260*, 89−94.

(38) Cheng, X.; Zhong, J.; Meng, J.; Yang, M.; Jia, F.; Xu, Z.; Kong, H.; Xu, H. Characterization of Multiwalled Carbon Nanotubes Dispersing in Water and Association with Biological Effects. *J. Nanomater.* **2011**, *2011*, 1−12.

(39) Tauc, J.; Grigorovici, R.; Vancu, A. Optical Properties and Electronic Structure of Amorphous Germanium. *Phys. Status Solidi* **1966**, *15*, 627−637.

(40) Mallick, P.; Sahoo, C. S. Effect of CuO Addition on the Structural and Optical Properties of NiO Nanoparticles. *Nanosci. Nanotechnol.* **2013**, *3*, 52−55.

(41) Davar, F.; Fereshteh, Z.; Salavati-Niasari, M. Nanoparticles Ni and NiO: synthesis, characterization and magnetic properties. *J. Alloys Compd.* **2009**, *476*, 797−801.

(42) Khan, J.; Ilyas, S.; Akram, B.; Ahmad, K.; Hafeez, M.; Siddiq, M.; Ashraf, M. A. Zno/NiO coated multi-walled carbon nanotubes for textile dyes degradation. *Arabian J. Chem.* **2018**, *11*, 880−896.

(43) Jorio, A.; Saito, R.; Dresselhaus, G.; Dresselhaus, M. S. Determination of nanotubes properties by Raman spectroscopy. *Philos. Trans. R. Soc., A* **2004**, *362*, 2311−2336.

(44) Sadezky, A.; Muckenhuber, H.; Grothe, H.; Niessner, R.; Poschl, U. Raman Microspectroscopy of Soot and Related Carbonaceous Materials: Spectral Analysis and Structural Information. *Carbon* **2005**, *43*, 1731−1742.

(45) Osswald, S.; Havel, M.; Gogotsi, Y. Monitoring oxidation of multiwalled carbon nanotubes by Raman spectroscopy. *J. Raman Spectrosc.* **2007**, *38*, 728−736.

(46) Qiao, H.; Wei, Z.; Yang, H.; Zhu, L.; Yan, X. Preparation and characterization of NiO nanoparticles by anodic arc plasma method. *J. Nano* **2009**, *2009*, 795928.

(47) Rakshit, S.; Ghosh, S.; Chall, S.; Mati, S. S.; Moulik, S. P.; Bhattacharya, S. C. Controlled synthesis of spin glass nickel oxide nanoparticles and evaluation of their potential antimicrobial activity: a cost effective and ecofriendly approach. *RSC Adv.* **2013**, *3*, 19348−19356.

(48) Amente, C.; Dharamvir, K. Purification and characterization of carbon nanotubes and the formation of magnetic semiconductors for the spintronic application. *Sci. Res.* **2015**, *3*, 122−128.

(49) Srivastava, N.; Srivastava, P. C. Realizing NiO nanocrystals from a simple chemical method. *Bull. Mater. Sci.* **2010**, *33*, 653−656.

(50) Yan, X.; Tong, X.; Wang, J.; Gong, C.; Zhang, M.; Liang, L. Synthesis of mesoporous NiO nanoflake array and its enhanced electrochemical performance for supercapacitor application. *J. Alloys Compd.* **2014**, *593*, 184−189.

(51) Ramoraswi, N. O.; Ndungu, P. G. Photo-catalytic properties of TiO$_2$ supported on MWCNTs, SBA-15 and Silica-coated MWCNTs nanocomposites. *Nanoscale Res. Lett.* **2015**, *10*, 427.

(52) Stein, J.; Lenczowski, B.; Frety, N.; Anglaret, E. Mechanical reinforcement of a high-performance aluminium alloy AA5083 with homogeneously dispersed multi-walled carbon nanotubes. *Carbon* **2012**, *50*, 2264−2272.

(53) Sheena, P. A.; Priyanka, K. P.; Sabu, N. A.; Sabu, B.; Varghese, T. Effect of calcination temperature on the structural and optical properties of nickel oxide nanoparticles. *Nanosyst.: Phys., Chem., Math.* **2014**, *5*, 441−449.

(54) Chiodarelli, N.; Richard, O.; Bender, H.; Heyns, M.; De Gendt, S.; Groeseneken, G.; Vereecken, P. M. Correlation between Number of Walls and Diameter in Multiwall Carbon Nanotubes Grown by Chemical Vapor Deposition. *Carbon* **2012**, *50*, 1748−1752.

(55) Shah, A.; Mao, Y. M.; Singh, L. R.; Gogoi, M.; Mahato, M. Waste plastic-derived FWCNT-NiMgAl composite for supercapacitor application. *Carbon Lett.* **2022**, *32*, 1541−1557.

(56) Zolfaghari, A.; Ataherian, F.; Ghaemi, M.; Gholami, A. Capacitive behavior of nanostructured MnO$_2$ prepared by sonochemistry method. *Electrochim. Acta* **2007**, *52*, 2806−2814.

(57) Xie, X.; Gao, L. Characterization of a manganese dioxide/carbon nanotube composite fabricated using an in situ coating method. *Carbon* **2007**, *45*, 2365−2373.

(58) Arunkumar, M.; Paul, A. Importance of Electrode Preparation Methodologies in Supercapacitor Applications. *ACS Omega* **2017**, *2*, 8039−8050.

(59) Lee, J. Y.; Liang, K.; An, K. H.; Lee, Y. H. Nickel oxide/carbon nanotubes nanocomposite for electrochemical capacitance. *Synth. Met.* **2005**, *150*, 153−157.

(60) Gao, B.; Yuan, C.-Z.; Su, L.-H.; Chen, L.; Zhang, X.-G. Nickel oxide coated on ultrasonically pretreated carbon nanotubes for supercapacitor. *J. Solid State Electrochem.* **2009**, *13*, 1251−1257.

(61) Sannasi, V.; Maheswari, K. U.; Karthikeyan, C.; Karuppuchamy, S. H2O2-assisted microwave synthesis of NiO/CNT nanocomposite material for supercapacitor applications. *Ionics* **2020**, *26*, 4067−4079.

(62) Su, A. D.; Zhang, X.; Rinaldi, A.; Nguyen, S. T.; Liu, H.; Lei, Z.; Lu, L.; Duong, H. M. Hierarchical porous nickel oxide−carbon nanotubes as advanced pseudocapacitor materials for supercapacitors. *Chem. Phys. Lett.* **2013**, *561−562*, 68−73.

(63) Mei, B.-A.; Munteshari, O.; Lau, J.; Dunn, B.; Pilon, L. Physical Interpretations of Nyquist Plots for EDLC Electrodes and Devices. *J. Phys. Chem. C* **2018**, *122*, 194−206.

(64) Vicentini, R.; Aguiar, J. P.; Beraldo, R.; Venâncio, R.; Rufino, F.; Da Silva, L. M.; Zanin, H. Ragone plots for electrochemical double-layer capacitors. *Batteries Supercaps* **2021**, *4*, 1291−1303.

(65) Zhao, G.; Li, Y.; Zhu, G.; Shi, J.; Lu, T.; Pan, L. Biomass-Based N, P, and S Self-Doped Porous Carbon for High-Performance Supercapacitors. *ACS Sustainable Chem. Eng.* **2019**, *7*, 12052−12060.

(66) Pal, B.; Yang, S.; Ramesh, S.; Thangadurai, V.; Jose, R. Electrolyte selection for supercapacitive devices: a critical review. *Nanoscale Adv.* **2019**, *1*, 3807−3835.

(67) Barve, A. K.; Gadegone, S. M.; Lanjewar, M. R.; Lanjewar, R. B. Synthesis and Characterization of Nickel Oxide based Nanocomposite Material. *Int. J. Eng. Res.* **2014**, 6−8.

(68) Mahato, M., Gogoi, M., Shah, A., Mandal, S. *The pyrolysis reactor apparatus and the process of MWCNT/H2 production using plastic waste*, 2022. India E-2/115/2022/KOL, (accessed April 21, 2022).